Peer-reviewed version available at Energies 2018, 11, 3086; doi:10.3390/en11113086

Article

CONTROL OF A DC-DC BUCK CONVERTER THROUGH CONTRACTION TECHNIQUES

David Angulo-García [1,‡*], Fabiola Angulo [2,†,‡], Gustavo Osorio [2,‡], and Gerard Olivar [3,]

1 Universidad de Cartagena. Instituto de Matemáticas Aplicadas. Grupo de Modelado Computacional - Dinámica y Complejidad de Sistemas. Carrera 6 # 36 - 100, Cartagena de Indias, Bolívar - Colombia. e-mail: dangulog@unicartagena.edu.co

2 Universidad Nacional de Colombia - Sede Manizales. Facultad de Ingeniería y Arquitectura. Departamento de Ingeniería Eléctrica, Electrónica y Computación. Percepción y Control Inteligente - Bloque Q, Campus La Nubia. Manizales, 170003 - Colombia. e-mail: {fangulog,gaosoriol}@unal.edu.co

3 Universidad Nacional de Colombia - Sede Manizales. Facultad de Ciencias Exactas y Naturales. Departamento de Matemáticas. Percepción y Control Inteligente - Bloque Q, Campus La Nubia. Manizales, 170003 - Colombia. e-mail: golivart@unal.edu.co

* Correspondence: dangulog@unicartagena.edu.co

Abstract: Reliable and robust control of power converters is a key issue in the performance of numerous technological devices. In this paper we show a design technique for the control of a DC-DC buck converter with a switching technique that guarantees not only good performance but also global stability. We show that making use of the contraction theorem in the Jordan canonical form of the buck converter, it is possible to find a switching surface that guarantees stability but it is incapable of rejecting load perturbations. To overcome this, we expand the system to include the dynamics of the voltage error and we demonstrate that the same design procedure is not only able to stabilize the system to the desired operation point but also to reject load, input voltage and reference voltage perturbations.

Keywords: DC-DC Buck Converter; Contraction Analysis; Global Stability; Matrix Norm

1. Introduction

Many industrial and residential applications use voltage regulation with DC-DC power converters; such applications include fuel cells [1], photovoltaic sources [2,3], control of DC motors [4], lighting appliances [5], computer power supplies [6], and many others. Power converters use a kind of non regulated voltage/current source (DC or AC) to convert to a regulated voltage/current one (DC or AC) that can be larger or lower than the initial one. Usually, the underlying structures in these devices are the so-called buck (step-down), boost (step-up), buck-boost (step down-step up), flyback, Ćuk, to mention few, depending on the type of application [7,8]. DC-DC power converters show both fast speed and capability of managing high power if needed [9]. More than 90% of the total amount of power supply in the world is processed through power converters [10]. For this reason, a precise control of these converters is a critical factor and therefore a vast amount of literature has been devoted to their control. For instance, PID-based schemes [11], Fuzzy PID control [12], robust controllers [13], predictive control [14], sliding mode control [15] and a controller based on a modified pulse-adjustment of the PWM [16], just to mention few.

The DC-DC buck power converter supplies a lower voltage than the input voltage and is one of the most studied power converters due to its simple design. The underlying topology of the buck converter is non-smooth as it switches back and forth according to a control signal, from continuous to discontinuous mode, to guarantee the required output voltage. Some examples of control techniques applied to the Buck converter include zero voltage control technique [17], fractional derivative control [18], controller based on active ramp tracking [19] and fuzzy PID controllers [20].

 doi:10.20944/preprints201809.0398.v1

Peer-reviewed version available at Energies 2018, 11, 3086; doi:10.3390/en11113086

Even though the effectiveness of these non-smooth control actions is out of doubt, usually the design of such controllers are based either on the averaged version of the system which effectively disregards the non-smoothness; or via linearization. This is because the effect of the nonlinearity is not always entirely understood and therefore the system can only be analyzed in the vicinity of the operation point (see [21] for a review on stability methods). This may result in undesired effects such as destabilization when the system is far from the operation point and limits the range of operation in which the DC-DC converter can work. This is because linearizing the system can only assure local stability, and the region of attraction is usually unknown.

Recently, a novel method to design an asymptotically globally stable controller for switched systems has been introduced in the literature [22,23] following the ideas of contraction theory, also used in [24]. Although some academic examples were shown using this theory [23], no examples of technological applications have been yet reported. In this paper, we propose to use these novel concepts to design a switched controller with applications to DC-DC power converters, specifically to the buck converter, such that the controlled system is asymptotically globally stable. With this purpose, the paper is organized as follows: In section 2 we present some preliminary concepts needed for the development of the paper, specifically on linear transformations, matrix measure, Filippov systems and contraction theory. After, in section 3, the buck power converter is presented as well as its principle of operation. In section 4, a controller based on contraction theory is designed and tested for the buck power converter. As the system is not robust, in section 5 we develop a modified control action that uses the principles of integral control which shows robustness preserving global stability. We conclude this paper with some remarks and future perspectives.

2. Mathematical methods

In this section we present some standard theory on linear systems (see [25]), matrix measures [26–28] and contraction theory applied to stability of switched systems [22,23] Most of the material can be found in the cited documents and references therein.

2.1. Linear transformations

Let us consider the piece-wise linear system (PWLS) given by

$$\dot{\mathbf{x}} = A\mathbf{x} + Bu\,, \tag{1}$$

where $u \in \{u_1,\ u_2\}$ and it commutes between booth values depending on the value of the switching surface $h(\mathbf{x})$=0. A is a Hurwitz matrix, the pair (A, B) is controllable and all eigenvalues are distinct but not necessarily real. Then, there exists a real matrix P which transforms the original system into a canonical form, so called the Jordan form, in the following way:

$$A_J = P^{-1}AP \qquad B_J = P^{-1}B\,. \tag{2}$$

The transformation matrix can be constructed as follows: For each real eigenvalue, its corresponding eigenvector is computed and assigned to one column of the matrix P. For every pair of complex eigenvalues their corresponding complex eigenvectors are computed but only one of them is used to construct two column vectors of the matrix P. The first one is composed by the real parts of the complex eignevector, while the other one is composed by the imaginary parts of the same eigenvector. For example, in a system with one real eigenvector $\mathbf{v}_1$ and two complex conjugate $\mathbf{v}_2$ and $\hat{\mathbf{v}}_2$ the matrix P takes the form

$$P = [\mathbf{v}_1 \quad \mathrm{Re}(\mathbf{v}_2) \quad \mathrm{Im}(\mathbf{v}_2)]\,. \tag{3}$$

Using this transformation matrix we obtain that every real eigenvalue $(\lambda_j = \eta_j)$ produces a column in the matrix A_J with the eigenvalue in the corresponding diagonal element with other elements equal

Preprints (www.preprints.org) | NOT PEER-REVIEWED | Posted: 20 September 2018 doi:10.20944/preprints201809.0398.v1

Peer-reviewed version available at Energies 2018, 11, 3086; doi:10.3390/en11113086

to zero. Every complex pair of eigenvalues ($\lambda_{k,k+1} = \alpha_k \pm \beta_k$) instead, generates a 2×2 block in the Jordan matrix such that the diagonal part corresponds to the real part of the eigenvalues and the other positions correspond to the positive and negative imaginay part: other elements are zero. A general example of this Jordan form is:

$$A_J = \begin{bmatrix} \eta_1 & 0 & 0 & 0 & 0 & 0 & \cdots \\ 0 & \ddots & 0 & 0 & 0 & 0 & \cdots \\ 0 & \cdots & \alpha_k & -\beta_k & 0 & 0 & \cdots \\ 0 & \cdots & \beta_k & \alpha_k & 0 & 0 & \cdots \\ 0 & \cdots & 0 & 0 & \alpha_{k+2} & -\beta_{k+2} & \cdots \\ 0 & \cdots & 0 & 0 & \beta_{k+2} & \alpha_{k+2} & \cdots \\ \vdots & \vdots & \vdots & \vdots & \vdots & \vdots & \ddots \end{bmatrix}. \quad (4)$$

2.2. Matrix measure

The norm-2 induced measure of a matrix A is defined as:

$$\mu_2(A) = \lambda_{\max}[A' + A]/2, \quad (5)$$

where $\lambda_{max}[\cdot]$ is the largest eigenvalue and A' is the transpose of A. It is possible to verify that, if the matrix A in (1) is Hurwitz, then $\mu_2(A_J)$ is always negative. This is an important issue in the stability analysis performed in this paper.

2.3. Contraction analysis for Filippov systems

Another way to define the system (1), is as a bimodal Filippov system

$$\dot{\mathbf{x}} = \begin{cases} F^+(\mathbf{x}) & \text{if } \mathbf{x} \in S^+ \\ F^-(\mathbf{x}) & \text{if } \mathbf{x} \in S^-. \end{cases} \quad (6)$$

where

$$F^+(\mathbf{x}) = A\mathbf{x} + Bu_1 \quad \text{and} \quad F^-(\mathbf{x}) = A\mathbf{x} + Bu_2$$

being

$$S^+ = \{\mathbf{x} \in \mathcal{U} : h(\mathbf{x}) > 0\} \quad \text{and} \quad S^- = \{\mathbf{x} \in \mathcal{U} : h(\mathbf{x}) < 0\}.$$

Here, $h : \mathcal{U} \to R$ is a smooth function called switching function and the surface Σ defined as

$$\Sigma = \{\mathbf{x} \in \mathcal{U} : h(\mathbf{x}) = 0\} \quad (7)$$

is called the switching surface.

According to [22,23], the bimodal Filippov system (6) is incrementally exponentially stable in a so-called K-reachable set $\mathcal{C} \subseteq \mathcal{U}$ with convergence rate $r = \min\{r_1, r_2\}$, if there exists some norm in $\mathcal{C}$ with associated measure μ such that for some positive constants r_1, r_2

$$\begin{aligned} \mu\left(\frac{\partial F^+(\mathbf{x})}{\partial \mathbf{x}}\right) &\leq -r_1 \qquad \forall \mathbf{x} \in \overline{S^+}, \\ \mu\left(\frac{\partial F^-(\mathbf{x})}{\partial \mathbf{x}}\right) &\leq -r_2 \qquad \forall \mathbf{x} \in \overline{S^-}, \end{aligned} \quad (8)$$

and

$$\mu((F^+(\mathbf{x}) - F^-(\mathbf{x})) \cdot \nabla h(\mathbf{x})) = 0 \qquad \forall \mathbf{x} \in \Sigma, \quad (9)$$

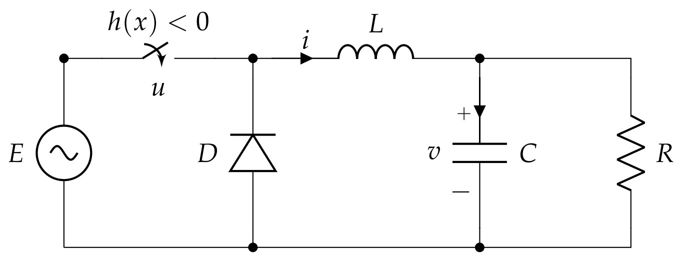

Figure 1. Schematic diagram of a buck power converter.

where $\overline{S^+}$ and $\overline{S^-}$ represent the closures of the sets S^+ and S^- respectively.

If system (6) is incrementally exponentially stable then there exist constants $k \geq 1$ and $\lambda > 0$ such that

$$|\mathbf{x}(t) - \mathbf{y}(t)| \leq ke^{-\lambda(t-t_0)}|\mathbf{x}(0) - \mathbf{y}(0)| \; \forall t \geq t_0 \; \forall \mathbf{x}(0), \mathbf{y}(0) \in \mathcal{C}$$

where $\mathbf{x}(t)$ and $\mathbf{y}(t)$ are solutions of the system. Thus we can establish global stability properties for system (1). Making use of the previous concepts, we will design an hybrid control for a buck power converter that guarantees not only global stability, but is also robust to different disturbances.

3. The buck power converter

The scheme of a buck power converter is depicted in Figure 1. The equations describing this dynamical system are

$$\begin{pmatrix} \dot{v} \\ \dot{i} \end{pmatrix} = \begin{pmatrix} -\frac{1}{RC} & \frac{1}{C} \\ -\frac{1}{L} & 0 \end{pmatrix} \begin{pmatrix} v \\ i \end{pmatrix} + \begin{pmatrix} 0 \\ \frac{E}{L} \end{pmatrix} u \tag{10}$$

where R is the load resistance, C is the capacitor's capacitance, L is the coil's inductance, and E is the voltage provided by the power source. The state variable v corresponds to the voltage across the capacitor and i quantifies the current flowing through the inductor. The control signal u takes values in the discrete set $\{0, \; 1\}$. When $u = 0$ the switch is opened and the power source (input voltage) does not feed the system. In this case, the load is being fed by the capacitor and the inductor. For simplicity we will perform a first transformation which maps the original system (10) into a dimensionless framework by means of the following similarity transformation $x = M^{-1}(v \; i)'$, where

$$M = \begin{pmatrix} E & 0 \\ 0 & \frac{E}{\sqrt{L/C}} \end{pmatrix} \tag{11}$$

Also we perform a normalization of the time as $\tau = t/\sqrt{LC}$, such that a new and unique parameter $\gamma = \frac{1}{R}\sqrt{\frac{L}{C}}$ holds the information of the parameters in the system. Therefore we can rewrite the equations as:

$$\begin{pmatrix} \dot{x}_1 \\ \dot{x}_2 \end{pmatrix} = \begin{pmatrix} -\gamma & 1 \\ -1 & 0 \end{pmatrix} \begin{pmatrix} x_1 \\ x_2 \end{pmatrix} + \begin{pmatrix} 0 \\ 1 \end{pmatrix} u \tag{12}$$

or in a compact form as $\dot{\mathbf{x}} = A\mathbf{x} + Bu$.

With the aim of designing the controller, it is necessary to transform the system to the Jordan normal form. As the pair (A, B) is controllable, then as outlined in Section 2.1, there exists a transformation matrix P given by

$$P = \begin{pmatrix} \gamma/2 & \rho \\ 1 & 0 \end{pmatrix} \tag{13}$$

Preprints (www.preprints.org) | NOT PEER-REVIEWED | Posted: 20 September 2018 doi:10.20944/preprints201809.0398.v1

Peer-reviewed version available at *Energies* **2018**, *11*, 3086; doi:10.3390/en11113086

which transforms the system into:

$$\begin{pmatrix} \dot{z}_1 \\ \dot{z}_2 \end{pmatrix} = \begin{pmatrix} -\gamma/2 & -\rho \\ \rho & -\gamma/2 \end{pmatrix} \begin{pmatrix} z_1 \\ z_2 \end{pmatrix} + \begin{pmatrix} 1 \\ -\gamma/(2\rho) \end{pmatrix} u \tag{14}$$

where $\mathbf{z} = P^{-1}\mathbf{x}$ and we have used $\rho := \rho(\gamma) = \sqrt{4-\gamma^2}/2$. These equations are noted in a compact form as $\dot{\mathbf{z}} = A_J \mathbf{z} + B_J u$.

4. Application to 2D-case

4.1. Controller design

Using the contraction theorem outlined in Sec. 2.3, we can establish that the converter operating with the switched signal control u will be stable if the following two conditions are satisfied:

$$\begin{aligned} &a)\mu_2(A_J) < -r_1 \ ,\forall \mathbf{z} \\ &b)\mu_2(B_J \cdot \nabla h(\mathbf{z})) = 0, \forall \mathbf{z} \in h(\mathbf{z}) = 0 \ . \end{aligned} \tag{15}$$

One can easily show that $\mu_2(A_J) = -\gamma/2$, hence condition a) is always met as γ is always positive. Then, considering $h(\mathbf{z})$ as a linear function of the states $h(\mathbf{z}) = (h_1 \ h_2) \cdot (z_1 \ z_2)'$, the condition b) can be written as:

$$\mu_2\left(\begin{pmatrix} 1 \\ -\gamma/(2\rho) \end{pmatrix} \cdot (h_1 \ h_2)\right) = 0 \ . \tag{16}$$

It is possible to demonstrate (see Appendix A) that the following choice of $h(\mathbf{z})$:

$$h(\mathbf{z}) \quad = \quad h_1 z_1 + \frac{B_J(2)}{B_J(1)} h_1 z_2 = (h_1 \ \ - h_1\gamma/(2\rho)) \cdot (z_1 \ z_2)' := h_z \cdot \mathbf{z} \,, \tag{17}$$

where $B_J(i)$ is the $i-th$ row element in B_J, fulfills condition (16) if the pairs $\{B_J(i), \ h(i)\}$ have opposite signs. Then, according to the signs of $B_J(i)$, it is necessary to choose $h_1 < 0$ and $h_2 > 0$. In this way, the matrix from which the maximum eigenvalue needs to be calculated according to Eq. (5), has one null eigenvalue and the other one can be computed as $\lambda_2 = h_1/\rho^2$, which is smaller than zero. Since the switching surface has been calculated in the canonical space, this result needs to be transformed back into the dimensionless state variables through $\mathbf{x} = P\mathbf{z}$. The switching manifold is then obtained as $h(\mathbf{x}) = h_z \cdot P^{-1} \cdot \mathbf{x}$, or equivalently:

$$h(\mathbf{x}) \quad = \quad (h_1 \quad h_1(1 + (\gamma/(2\rho))^2) \cdot (x_1 \quad x_2)' := h_x \cdot \mathbf{x} \tag{18}$$

Of course, the term h_x correspond the vector in the normal direction of the switching surface. With the aim of simplifying the calculations we normalize such vector such that $|h_x| = 1$. Moreover, we need to subtract the reference values to the states to ensure the regulation to the operation point.

$$h(\mathbf{x}) \quad = \quad \left(-\frac{\gamma}{\sqrt{4+\gamma^2}} \quad \frac{2}{\sqrt{4+\gamma^2}}\right) \cdot (x_1 - \bar{x}_{1ref} \quad x_2 - \bar{x}_{2ref})' = 0 \ . \tag{19}$$

Finally, we can define the switching manifold in terms of the original state variables $(x_1 \ x_2) = M^{-1}(v \ i)'$ leading to:

$$h(v,i) \quad = \quad \left(-\frac{\gamma}{E\sqrt{4+\gamma^2}} \quad \frac{2\sqrt{L/C}}{E\sqrt{4+\gamma^2}}\right) \cdot (v - \bar{v}_{ref} \quad i - \bar{i}_{ref})' = 0 \ . \tag{20}$$

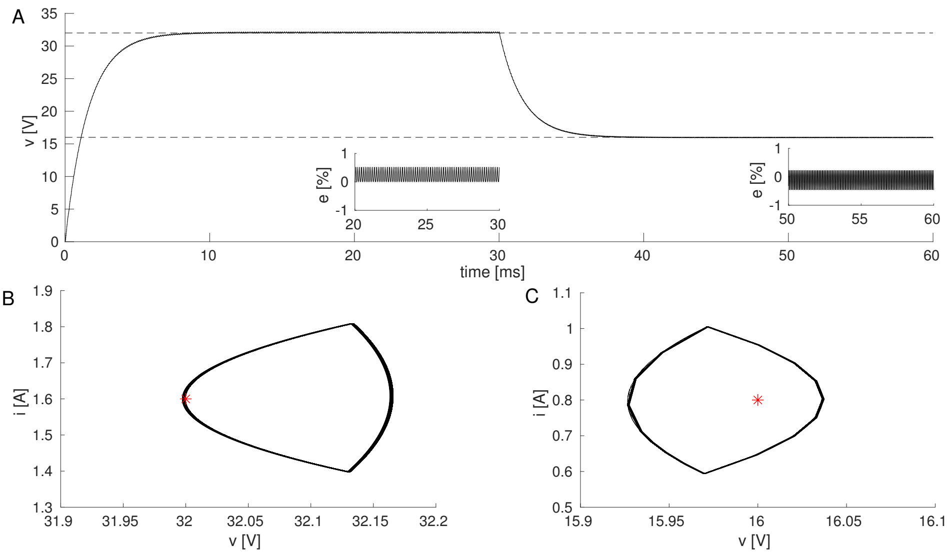

Figure 2. A) Time trace of the voltage in the capacitor v. During the first 30ms a $\bar{v}_{ref} = 32$V is used, after this a drastic change to $\bar{v}_{ref} = 16$V is applied (depicted in the dashed lines). The time trace of the steady state percentage error is also depicted in the insets for both values of $\bar{v}_{ref}$. B) Phase representation of the steady state for $\bar{v}_{ref} = 32$ and C) $\bar{v}_{ref} = 16$, with the equilibrium point indicated by the red star. Simulations were performed with an RK4 algorithm with event detection to identify collisions with the hysteresis band. Steady state was considered after 20ms of simulation time. Initial conditions were chosen as $(v, i) = (0, 0)$. Other parameters as in the main text.

It is worth noticing that neither h_1 nor h_2 appear in the calculations. On the one hand h_2 is parametrized via h_1 (see appendix A), on the other hand h_1 disappear via the normalization, reducing effectively two degrees of freedom.

4.2. Simulation results

Unless otherwise stated we will use the following set of parameters for numerical computations: $R = 20\Omega$, $L = 2$mH, $C = 40\mu$F, $E = 40$V and $\bar{v}_{ref} = 32$V. The desired current reference can be assumed to be $\bar{i}_{ref} = \bar{v}_{ref}/R = 1.6$A. With this, $\gamma \approx 0.35$ and $\rho \approx 0.98$. Also, as electronic devices cannot switch with infinite speed, it is necessary to implement a hysteresis band for simulating the change in the position of the MOSFET. We have designed this band in such a way that the switching time is close to 175μs. Under these assumptions, Eq. (20) takes the following values:

$$h(v, i) = \begin{pmatrix} -4.4 \times 10^{-3} & 0.1741 \end{pmatrix} \cdot \begin{pmatrix} v - \bar{v}_{ref} & i - \bar{i}_{ref} \end{pmatrix}' \pm 0.02 \quad (21)$$

In Fig. 2 we show the performance of the designed control. In particular, in Fig. 2A) the time trace of the voltage v is depicted in response to a drastic change in the reference output voltage $\bar{v}_{ref}$. During the first 30ms, where the system is subject to $\bar{v}_{ref} = 32$V (top dashed line), the output voltage reaches the steady state close to 5.7ms, with no overshoot and the maximum error in steady state is lower than 0.6% (see inset). After 30ms, the reference voltage is changed to $\bar{v}_{ref} = 16$V (bottom dashed line) and the system is able to track the change and stabilize to the new value of output voltage. In Fig. 2B) and C) we plot the orbit in the (v, i) space during the steady state for the two references used in panel A) of the same figure. From this, one can observe that indeed the equilibrium value $(\bar{v}_{ref}, \bar{i}_{ref})$ is reached through the continuous rippling of the orbit around the equilibrium point (red symbol).

Peer-reviewed version available at Energies 2018, 11, 3086; doi:10.3390/en11113086

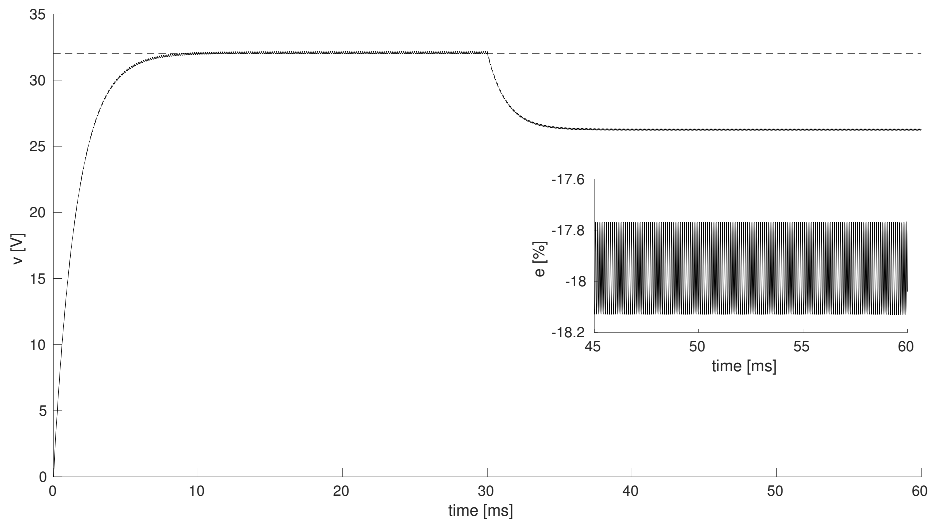

Figure 3. Time response of the capacitor's voltage v. During the first 30ms, the value of the resistor is set to $R = 20\Omega$, after this the load is changed to $R = 18\Omega$. Inset: Steady state percentage error (considered 15ms after the presentation of the disturbance). The desired output is plot with the dashed line. Other details as in Fig. 2.

We also tested the robustness of the control to changes in the load. In Fig. 3 is depicted the time trace of the voltage in this scenario. Following a similar procedure as in Fig. 2, after 30ms, a change in the resistance from $R = 20\Omega$ to $R = 15\Omega$ (10% difference) is applied. From this figure it is possible to see that the system drifts away from the reference output $\bar{v}_{ref} = 32$V (dashed line), producing a steady state error of around 18% (see inset).

So far, the controller designed with contraction theory has been successful to operate in a desired way and reject disturbances in the output voltage. However, when a disturbance in the load is presented (a common situation in power converters) the system loses the ability to follow the desired output voltage, indicating that the controller is not robust. To solve this problem, we extend the proposed controller based on the idea of an integral control action.

5. Application to 3D-case

5.1. Controller design based on a modified integral control action

In control theory it is known that perturbations are better rejected by a PI controller; however, in this case, adding a PI controller implies to add a pole in the origin of the system which prevents us from applying contraction theorem. Then, with the aim of enhancing the robustness of the controlled system, we will modify the control action in such a way that it introduces the dynamics of the error. To do so we introduce a new state variable x_3 in the dimensionless system in the following way: $\dot{x}_3 = e - \delta x_3$, with $e = \bar{x}_{1ref} - x_1$ defined as the output error and δ as the time constant of x_3. As $x_1 = v/E$, then $\bar{x}_{1ref} = \bar{v}_{ref}/E$. Under these assumptions, the system takes the following form:

$$\begin{pmatrix} \dot{x}_1 \\ \dot{x}_2 \\ \dot{x}_3 \end{pmatrix} = \begin{pmatrix} -\gamma & 1 & 0 \\ -1 & 0 & 0 \\ -1 & 0 & -\delta \end{pmatrix} \begin{pmatrix} x_1 \\ x_2 \\ x_3 \end{pmatrix} + \begin{pmatrix} 0 \\ 1 \\ 0 \end{pmatrix} u + \begin{pmatrix} 0 \\ 0 \\ 1 \end{pmatrix} \bar{x}_{1ref} \tag{22}$$

with

Peer-reviewed version available at Energies 2018, 11, 3086; doi:10.3390/en11113086

$$u = \begin{cases} 1 & \text{if } h(\mathbf{x}) \leq 0 \\ 0 & \text{otherwise.} \end{cases} \tag{23}$$

or in compact form $\dot{\mathbf{x}} = A\mathbf{x} + Bu + Q\bar{x}_{1ref}$. The aim of the term $-\delta$ appearing in position $\{3,3\}$ in the matrix A is to stabilize the system allowing us to apply the contraction theorem. In this way, the value of δ must be very small to avoid high steady state error. As the pair (A, B) is controllable we then proceed to apply the general theory with a new consideration: In the construction of the matrix P we will take into account the norm of the eigenvectors $\mathbf{v}_i$, which will allow us to gain more degrees of freedom in the system to tune the controller. Indeed this is not an issue when obtaining the canonical form A_J as the operation $P^{-1}AP$ cancels out any norm that may have been considered. However, the transformed matrix B_J, which is critical for the stability conditions Eq. (15), may depend on the chosen modules of the eigenvectors. To take this into account, we need to include in Eq. (3) the magnitude of the eigenvectors via the scaling factors c_1 and c_2 as follows:

$$P = \left[c_1\mathbf{v}_1 \quad c_2\mathrm{Re}(\mathbf{v}_2) \quad c_2\mathrm{Im}(\mathbf{v}_2)\right]. \tag{24}$$

The general form of the transformation matrix can then be written as

$$P = \begin{pmatrix} 0 & c_2(\gamma - 2\delta)/2 & -c_2\rho \\ 0 & c_2(2 - \gamma\delta)/2 & -c_2\rho\delta \\ c_1 & c_2 & 0 \end{pmatrix} \tag{25}$$

which leads to the transformed system $\dot{\mathbf{z}} = A_J\mathbf{z} + B_J u + Q_J\bar{x}_{1ref}$, where

$$\begin{aligned} A_J &= \begin{pmatrix} -\delta & 0 & 0 \\ 0 & -\gamma/2 & \rho \\ 0 & -\rho & -\gamma/2 \end{pmatrix} \\ B_J &= \begin{pmatrix} -1/(c_1(\delta^2 - \gamma\delta + 1)) \\ 1/(c_2(\delta^2 - \gamma\delta + 1)) \\ -(2\delta - \gamma)/(2c_2\rho(\delta^2 - \gamma\delta + 1)) \end{pmatrix} \\ Q_J &= \begin{pmatrix} 1 & 0 & 0 \end{pmatrix}' \end{aligned} \tag{26}$$

The purpose will be again to find a switching function $h(\mathbf{z}) = h_1z_1 + h_2z_2 + h_3z_3$ that meets the conditions of global stability in Eq. (15) in the transformed space. One can easily verify that, provided that $\delta < \gamma/2$, $\mu(A_J) = -\gamma/2$, fulfilling condition a). Moreover, one of the eigenvalues of $B_J \cdot \nabla h(\mathbf{z})$ is always 0 due to the fact that the matrix is constructed using only two linearly independent vectors (see Appendix A.2). Also, following a similar procedure as in the 2D case, choosing the following switching function :

$$h(\mathbf{z}) = h_1z_1 + \frac{B_J(2)}{B_J(1)}h_1z_2 + \frac{B_J(3)}{B_J(1)}h_1z_3, \tag{27}$$

the condition b) in Eq. (9) is always guaranteed if, for every pair $\{B_J(i),\ h(i)\}$, its elements have opposite signs and the signs of c_1 and h_1 are equal (see appendix A) . From this, the switching surface in the canonical space is:

$$h(\mathbf{z}) = \begin{pmatrix} h_1 & -h_1\dfrac{c_1}{c_2} & h_1\dfrac{c_1(2\delta - \gamma)}{2c_2\rho} \end{pmatrix} \cdot (z_1\ \ z_2\ \ z_3)' := h_z \cdot \mathbf{z} \tag{28}$$

It is worth noticing that for the 2D case, considering arbitrary norms for the eigenvectors does not have an effect in the possible switching functions, in contrast to the extended system. This is because there is only one constant associated to that norm (two complex eigenvalues). Another important

Preprints (www.preprints.org) | NOT PEER-REVIEWED | Posted: 20 September 2018 doi:10.20944/preprints201809.0398.v1

Peer-reviewed version available at *Energies* **2018**, *11*, 3086; doi:10.3390/en11113086

aspect is that the plane defined in Eq. (28) depends on the ratio c_1/c_2 and not on their individual values which effectively reduces one degree of freedom in the tunning parameters of the hybrid controller based on the integral action. As in the previous case, the next steps in the design are i) apply the transformation to the dimensionless variables; ii) normalize by the norm of the resulting orthogonal vector to the switching surface in the **x** space, i.e. $|h_z \cdot P^{-1}|$; and iii) transform back to the original buck converter states variables $(v,\ i)$ via the matrix M (recall that the similarity transformation is $x = M^{-1}(v\ i)'$). It is important to notice that for the 3D system, the matrix M is not unique, as we don't know the exact mapping between the extended variable x_3 and its counterpart in the real system y. We can assume without loss of generality and preserving the idea of the integral action, that the mapping between x_3 and y is given by a scaling factor, which after some algebra can be demonstrated to be $x_3 = y/(E\sqrt{LC})$. This results preserves the information of the error defined by $\bar{v}_{ref}$. The similarity transformation matrix is then given by:

$$M = \begin{pmatrix} E & 0 & 0 \\ 0 & E/\sqrt{L/C} & 0 \\ 0 & 0 & E\sqrt{LC} \end{pmatrix} . \tag{29}$$

We will avoid displaying the rather long expression of performing the aforementioned steps, but they can be summarized in the operation:

$$h(v,i,y) = \frac{h_z \cdot P^{-1}}{|h_z \cdot P^{-1}|} \cdot M^{-1}(v \quad i \quad y)' . \tag{30}$$

The system finally reads in its original variables as:

$$\begin{pmatrix} \dot{v} \\ \dot{i} \\ \dot{y} \end{pmatrix} = \begin{pmatrix} -\frac{1}{RC} & \frac{1}{C} & 0 \\ -\frac{1}{L} & 0 & 0 \\ -1 & 0 & -\frac{\delta}{\sqrt{LC}} \end{pmatrix} \begin{pmatrix} v \\ i \\ y \end{pmatrix} + \begin{pmatrix} 0 \\ E/L \\ 0 \end{pmatrix} u + \begin{pmatrix} 0 \\ 0 \\ 1 \end{pmatrix} \bar{v}_{ref} \tag{31}$$

with

$$u = \begin{cases} 1 & \text{if } h(v,i,y) \leq 0 \\ 0 & \text{otherwise.} \end{cases} \tag{32}$$

5.1.1. Simulation results

From Eqs. (30) and (31), the resulting controlled system can be tuned via two parameters, namely the time constant of the extended variable δ, and the ratio c_1/c_2 of the norm of the eigenvectors associated with matrix A. To tune these parameters, we performed an optimization routine which explored several possible combinations of parameters δ and c_1/c_2 in a wide range of values. Following an heuristic approximation we chose the values which met some desired criteria, namely small overshoot and small settling time. From this analysis we concluded that a sufficiently small value of δ is necessary in order for the steady state error to be small. Also, as c_1/c_2 is decreased, the system evolves faster but produces large overshoots; conversely, increasing the ratio reduces the overshoot but slows down the system. A good performance was achieved by choosing $\delta = 1 \times 10^{-4}$ and $c_1/c_2 = 9$. With these choices, the numerical values for the switching surface are:

$$h(v,i,y) = \left(-4.3 \times 10^{-3} \quad 0.1741 \quad -1.03\right) \cdot (v \quad i \quad y)' \pm 0.05 , \tag{33}$$

where we have set the hysteresis to a value that meets the MOSFET switching frequency criterion as in the previous section. It can be noted that this controller does not require any information about current reference as in 2D-case.

Peer-reviewed version available at Energies 2018, 11, 3086; doi:10.3390/en11113086

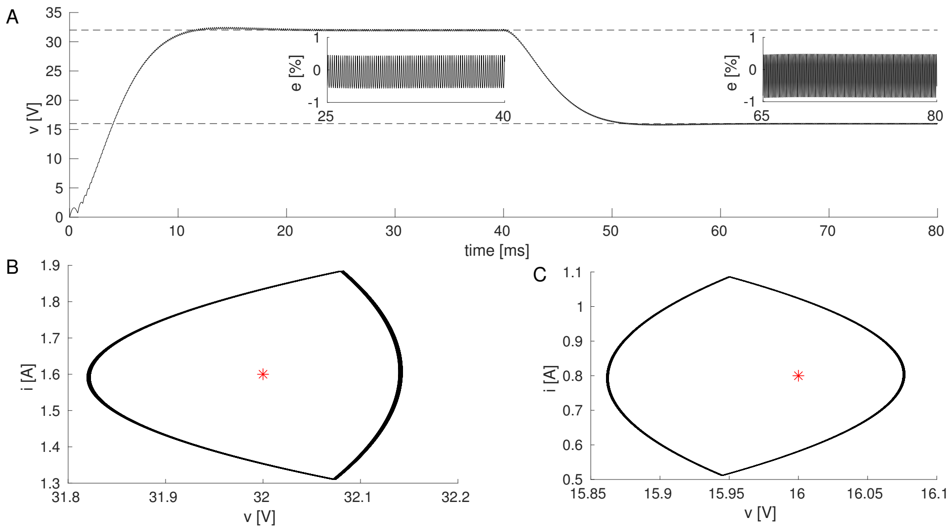

Figure 4. A) Time trace of the voltage in the capacitor v. During the first 40ms a $\bar{v}_{ref} = 32$V is used, after this a drastic change to $\bar{v}_{ref} = 16$V is applied (depicted in the dashed lines). The time trace of the steady state percentage error is also depicted in the insets for both values of $\bar{v}_{ref}$. B) Phase representation of the steady state for $\bar{v}_{ref} = 32$ and C) $\bar{v}_{ref} = 16$, with the equilibrium point indicated by the red star. This results were obtained by making $c_1/c_2 = 9$ and $\delta = 1 \times 10^{-4}$. Steady state was considered after 25ms of transient dynamics. Other parameters as in the main text and Fig. 2.

The results of the 3D system behavior and its ability to reject disturbances in the reference voltage are depicted in Figure 4. In this figure, a reference voltage of $\bar{v}_{ref} = 32$V is applied during the first 40ms of the simulation, after this, the reference voltage is drastically decreased by a 50%, i.e $\bar{v}_{ref} = 16$V and the system is allowed to evolve during 40ms more. From Fig. 4A) it is possible to deduce that, in the 3D system, the controller is also able to regulate with a settling time of $\approx$ 10ms and a steady state error smaller than 1%. Not only this, but also the control is robust against disturbances in the reference output value. Panels B) and C) of the same figure show the orbit exhibited by the system in the steady state before and after the disturbance, which clearly evolves in the neighborhood of the equilibrium value $(\bar{v}_{ref}, \bar{i}_{ref})$ (red star).

We also tested the capability of the system to reject disturbances both in the load R and the input voltage E. To do so we simulated a similar set-up to the one described for the 2D system. In particular we evolved the unperturbed system during 40ms to achieve a steady state, and immediately after the perturbation is presented. For Fig. 5A) the perturbation is induced as a sudden change in the load from $R = 20\Omega$ to $R = 15\Omega$ (25% change). As depicted in the main figure of the panel and its inset, the system recovers to the reference voltage $\bar{v}_{ref} = 32$V (dashed line) with a percentage error smaller than 1%. A similar scenario is plotted in Fig 5B), in this case the perturbation is presented as a change in the input voltage from $E = 40$V to $E = 50$V. Even though the perturbation in the input corresponds to a 25% change, the system doesn't drift away from the equilibrium point.

It should be noticed that the first two elements in the normal vector of the switching surface in Eq. (33), are exactly those of Eq. (21) for the 2D case, where neither the norm of the vectors nor δ were involved. Hence, the effect of c_1/c_2 and δ are only exhibited in the third term.

6. Conclusions

In this paper a stable hybrid control technique was designed and analyzed in a buck power converter, applying results from contraction analysis which make use of the induced matrix measure.

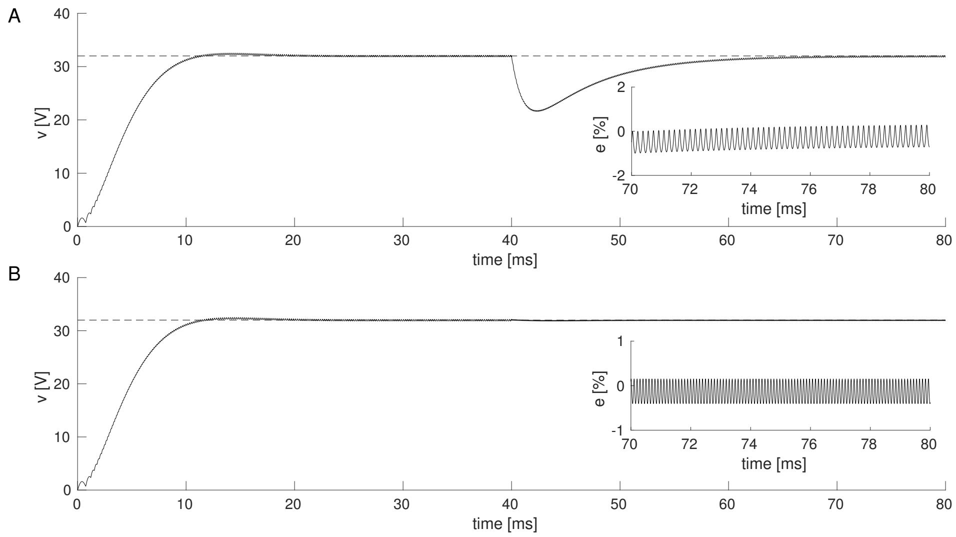

Figure 5. A) Time response of the capacitor's voltage v. During the first 40ms, the value of the resistor is set to $R = 20\Omega$, after this the load is changed to $R = 15\Omega$. Insets: Steady state percentage error (considered 25ms after the presentation of the disturbance). The desired output is plot with the dashed line. B) Same as A) for a disturbance in the input voltage E. During the first 40ms $E = 40$V, after this it is changed to $E = 50$V. Other details as in Fig. 2.

We took advantage of the Jordan canonical form of the system to guarantee the conditions of stability resulting from contraction analysis, which wouldn't have been met in the original form of the system. For the original 2D buck converter, two reference points $\bar{x}_{1ref}$ and $\bar{x}_{2ref}$ were introduced in the switching function to allow for regulation to the desired state. Under these conditions, the controller presented good performance and robustness to voltage reference change, however, as the load varies, regulation is lost. To overcome this issue we extended the system to take into account the dynamics of the error, in a similar similar way to the design of a PI controller. With this design, the controlled system showed robustness to several types of disturbances including load and input voltage changes.

Although the 3D system is robust, it comes with the price of increasing the settling time to around 10ms. Other controllers applied to the buck converter may show better performance in this particular matter. Nonetheless it should be stressed that the method outlined in this paper is not based on the linearized system but on the nonlinear form, such that the final controller is globally stable which cannot be guaranteed using linearization. Indeed we have numerically tested the globally stability property by performing extensive simulations for different initial conditions in the (v, i, y) space. These tests showed convergence for all the simulations.

For the sake of simplifying the calculations we have considered throughout this manuscript a switching function with zero offset. Introducing the offset in this function, which amounts to perform a translation of the switching surface, does not change any of the stability criteria that we have presented here, but it could certainly serve as a further tunning parameter of the controller. A general direction is to choose the offset in such a way that the trajectory of the system enters in sliding mode as early as possible.

The analytic results presented here hold for the theoretical set-up in which perfect sliding over the switching manifold is allowed. Realistically speaking this is unachievable due to the finite frequency of the MOSFET used to implement the switching action, and therefore we are constrained to include in the simulations a hysteresis band which allows for finite switching frequencies. The size of the hysteresis band is an important issue because its width determines the size of the chattering in the voltage variable.

Preprints (www.preprints.org) | NOT PEER-REVIEWED | Posted: 20 September 2018 doi:10.20944/preprints201809.0398.v1

Peer-reviewed version available at Energies 2018, 11, 3086; doi:10.3390/en11113086

Finally, whether the approach presented here can be applied to other power converters such as the Boost, is currently an open problem. This is because not every single system can be easily approached by contraction theory and other standard tools for stability analysis might be the best option in these cases.

Author Contributions: "Conceptualization was made by F.A. and D.A-G.; Supervision and Project Administration were made by F.A., Gu.O and Ge.O.; Software and Validation and Funding Acquisition by D.A-G, F.A. and Gu.O.; Visualization made by D.A-G and Gu.O. All authors contributed to Formal Analysis, Investigation and Writing."

Funding: F.A and Gu.O were supported by Universidad Nacional de Colombia, Manizales, Project 31492 from Vicerrectoría de Investigación, DIMA, and COLCIENCIAS under Contract FP44842-052-2016. D.A-G was supported by Universidad de Cartagena through the "Novena Convocatoria de Proyectos de Investigación".

Conflicts of Interest: The authors declare no conflict of interest. The founding sponsors had no role in the design of the study; in the collection, analyses, or interpretation of data; in the writing of the manuscript, and in the decision to publish the results.

Appendix A

In this appendix we prove that, for a particular selection of the constants h_i, $\mu_2(B \cdot \nabla h(\mathbf{x})) := \mu_2(B \cdot h) \leq 0$.

Appendix A.1 Matrix measure for a 2D system

Without loss of generality, we can consider two vectors $B = [b_1 \;\; b_2]'$ and $h = [h_1 \;\; h_2]$. The matrix N is formed as

$$N = B \cdot h + h' \cdot B' .$$

The measure of this matrix must be equal to zero over the switching surface to meet the theorem in [22,23]. As this matrix is symmetric, then:

$$\mu_2(N) = \lambda_{\max}[N' + N]/2 = \lambda_{\max}[N] = 0 \tag{A1}$$

This condition is equivalent to the matrix N being negative semidefinite, or the matrix $-N$ being positive semidefinite, i.e.

$$\lambda_{\min}[-N] = 0$$

An extensive discussion about positive definiteness can be found in [25,26]. Then, the conditions associated with the eigenvalues can be computed using theory of positive definite matrices which states that in a symmetric matrix all its eigenvalues are greater than zero if and only if all its principal minors are positive. This matrix is called positive definite. A matrix is positive semidefinite if all its eigenvalues are greater than or equal to zero. On the other hand, a matrix N is negative semidefinite if $-N$ is positive semidefinite.

In this way, the matrix N is given by:

$$N = \begin{pmatrix} 2b_1h_1 & b_1h_2 + b_2h_1 \\ b_1h_2 + b_2h_1 & 2b_2h_2 \end{pmatrix}. \tag{A2}$$

To fulfill the condition to be negative semidefinite, we have to check that all principal minors of $-N$ are greater than or equal to zero ($\Delta_k \geq 0$)

First order principal minors. The matrix has two first order principal minors which are:

$$M_1^1(-N) := \Delta_{11}(-N) = -N_{11} = -2b_1h_1 \geq 0 \tag{A3}$$

Preprints (www.preprints.org) | NOT PEER-REVIEWED | Posted: 20 September 2018 doi:10.20944/preprints201809.0398.v1

Peer-reviewed version available at Energies 2018, 11, 3086; doi:10.3390/en11113086

and

$$M_1^2(-N) := \Delta_{12}(-N) = -N_{22} = -2b_2h_2 \geq 0 \tag{A4}$$

As it can be seen, the only condition is that the pairs $\{b_i,\ h_i\}$ have opposite signs.

Second order principal minors. This system has only one second order principal minor which is computed as:

$$\Delta_2^1(-N) = det \begin{pmatrix} -2b_1h_1 & -b_1h_2 - b_2h_1 \\ -b_1h_2 - b_2h_1 & -2b_2h_2 \end{pmatrix} \geq 0$$

From this inequality is obtained:

$$b_1h_2 = b_2h_1 \tag{A5}$$

Supposing h_1 as a free parameter to tune, it is obtained that:

$$h_2 = \frac{b_2}{b_1}h_1 \tag{A6}$$

Replacing A6 in A4 it can be seen that independently of the value and sign of b_2 the inequality is satisfied.

The proof is complete.

Appendix A.2 Measure matrix for 3D system

Following the ideas of previous section, N is given by:

$$N = \begin{pmatrix} 2b_1h_1 & b_1h_2 + b_2h_1 & b_1h_3 + b_3h_1 \\ b_1h_2 + b_2h_1 & 2b_2h_2 & b_2h_3 + b_3h_2 \\ b_1h_3 + b_3h_1 & b_2h_3 + b_3h_2 & 2b_3h_3 \end{pmatrix} \tag{A7}$$

To fulfill the condition to be negative semidefinite, we have to check that all principal minors of $-N$ are greater than or equal to zero ($\Delta_k \geq 0$)

First order principal minors. Here, there are three first order principal minors, they are:

$$M_1^1(-N) := \Delta_{11}(-N) = -N_{11} = -2b_1h_1 \geq 0 \tag{A8}$$

$$M_1^2(-N) := \Delta_{12}(-N) = -N_{22} = -2b_2h_2 \geq 0 \tag{A9}$$

and

$$M_1^3(-N) := \Delta_{13}(-N) = -N_{33} = -2b_3h_3 \geq 0 \tag{A10}$$

As it can be seen, the only condition is that the pairs $\{b_i,\ h_i\}$ have opposite signs.

Second order principal minor. In this case, there are three second order principal minors. The first one is:

$$\Delta_2^1(-N) = det \begin{pmatrix} -2b_2h_2 & -b_2h_3 - b_3h_2 \\ -b_2h_3 - b_3h_2 & -2b_3h_3 \end{pmatrix} \geq 0$$

After some computations the following equation is obtained.

$$b_2h_3 = b_3h_2 \tag{A11}$$

Other second order principal minor is given by:

$$\Delta_2^2(-N) = det \begin{pmatrix} -2b_1h_1 & -b_1h_3 - b_3h_1 \\ -b_1h_3 - b_3h_1 & -2b_3h_3 \end{pmatrix} \geq 0$$

As in previous case, it is obtained:

$$b_1h_3 = b_3h_1 \tag{A12}$$

The last second order principal minor is computed as:

$$\Delta_2^3(-N) = det \begin{pmatrix} -2b_1h_1 & -b_1h_2 - b_2h_1 \\ -b_1h_2 - b_2h_1 & -2b_2h_2 \end{pmatrix} \geq 0$$

and in a similar way it is obtained:

$$b_1h_2 = b_2h_1 \tag{A13}$$

Taking into account these three inequalities and considering h_1 as a free parameter to tune, it is obtained from A13

$$h_2 = \frac{b_2}{b_1}h_1$$

From A12

$$h_3 = \frac{b_3}{b_1}h_1$$

To finally prove from A11 that h_3 takes the same value as already given. Replacing these values in expressions A8 to A10, the equalities still are preserved regardless of the value and sign of constants b_i.

Third order principal minor. As matrix N is obtained from two vectors, its range cannot be greater than two, then its third order principal minor namely

$$\Delta_3^1(-N) = det(-N) = 0$$

The proof is complete.

References

1. Chen, S.M.; Wang, C.Y.; Liang, T.J. A novel sinusoidal boost-flyback CCM/DCM DC-DC converter. 2014 IEEE Applied Power Electronics Conference and Exposition - APEC 2014; , 2014; pp. 3512–3516.
2. Tseng, K.C.; Lin, J.T.; Cheng, C.A. An Integrated Derived Boost-Flyback Converter for fuel cell hybrid electric vehicles. 2013 1st International Future Energy Electronics Conference (IFEEC); , 2013; pp. 283–287.
3. Siouane, S.; Jovanovic, S.; Poure, P. Service Continuity of PV Synchronous Buck/Buck-Boost Converter with Energy Storage. *Energies* **2018**, *11*. doi:10.3390/en11061369.
4. Ortigoza, R.S.; Rodriguez, V.H.G.; Marquez, E.H.; Ponce, M.; Sanchez, J.R.G.; Juarez, J.N.A.; Ortigoza, G.S.; Perez, J.H. A Trajectory Tracking Control for a Boost Converter-Inverter-DC Motor Combination. *IEEE Latin America Transactions* **2018**, *16*, 1008–1014.
5. Fernando, W.A.; Lu, D.D. Bi-directional converter for interfacing appliances with HFAC enabled power distribution systems in critical applications. 2017 20th International Conference on Electrical Machines and Systems (ICEMS), 2017, pp. 1–6. doi:10.1109/ICEMS.2017.8056490.
6. Singh, S.; Singh, B.; Bhuvaneswari, G.; Bist, V. A Power Quality Improved Bridgeless Converter-Based Computer Power Supply. *IEEE Transactions on Industry Applications* **2016**, *52*, 4385–4394. doi:10.1109/TIA.2016.2575365.
7. Undeland, T.M.; Robbins, W.P.; Mohan, N. *Power electronics: converters, applications, and design*; New York: John Wiley and Sons, 2003.
8. Erickson, R.W.; Maksimović, D. *Fundamentals of Power Electronics*; Springer, 2001.

Preprints (www.preprints.org) | NOT PEER-REVIEWED | Posted: 20 September 2018 doi:10.20944/preprints201809.0398.v1

Peer-reviewed version available at *Energies* **2018**, *11*, 3086; doi:10.3390/en11113086

9. Mueller, J.A.; Kimball, J. Modeling Dual Active Bridge Converters in DC Distribution Systems. *IEEE Transactions on Power Electronics* **2018**, pp. 1–1. doi:10.1109/TPEL.2018.2867434.
10. Banerjee, S.; Verghese, G., Eds. *Nonlinear Phenomena in Power Electronics*; IEEE Press, 2001.
11. Cheng, C.H.; Cheng, P.J.; Xie, M.J. Current sharing of paralleled DC–DC converters using GA-based PID controllers. *Expert Systems with Applications* **2010**, *37*, 733 – 740. doi:https://doi.org/10.1016/j.eswa.2009.05.083.
12. Guo, L.; Hung, J.Y.; Nelms, R.M. Evaluation of DSP-Based PID and Fuzzy Controllers for DC-DC Converters. *IEEE Transactions on Industrial Electronics* **2009**, *56*, 2237–2248.
13. Rodríguez-Licea, M.A.; Pérez-Pinal, F.J.; Nuñez-Perez, J.C.; Herrera-Ramirez, C.A. Nonlinear Robust Control for Low Voltage Direct-Current Residential Microgrids with Constant Power Loads. *Energies* **2018**, *11*. doi:10.3390/en11051130.
14. Aguilera, R.P.; Quevedo, D.E. Predictive Control of Power Converters: Designs With Guaranteed Performance. *IEEE Transactions on Industrial Informatics* **2015**, *11*, 53–63. doi:10.1109/TII.2014.2363933.
15. Alsmadi, Y.M.; Utkin, V.; Haj-ahmed, M.A.; Xu, L. Sliding mode control of power converters: DC/DC converters. *International Journal of Control* **2017**, *0*, 1–22, [https://doi.org/10.1080/00207179.2017.1306112]. doi:10.1080/00207179.2017.1306112.
16. Khaligh, A.; Rahimi, A.M.; Emadi, A. Modified Pulse-Adjustment Technique to Control DC/DC Converters Driving Variable Constant-Power Loads. *IEEE Transactions on Industrial Electronics* **2008**, *55*, 1133–1146. doi:10.1109/TIE.2007.909757.
17. Chiang, C.; Chen, C. Zero-Voltage-Switching Control for a PWM Buck Converter Under DCM/CCM Boundary. *IEEE Transactions on Power Electronics* **2009**, *24*, 2120–2126. doi:10.1109/TPEL.2009.2021186.
18. Calderón, A.; Vinagre, B.; Feliu, V. Fractional order control strategies for power electronic buck converters. *Signal Processing* **2006**, *86*, 2803–2819. Special Section: Fractional Calculus Applications in Signals and Systems, doi:https://doi.org/10.1016/j.sigpro.2006.02.022.
19. Suh, J.; Seok, J.; Kong, B. A Fast Response PWM Buck Converter with Active Ramp Tracking Control in Load Transient period. *IEEE Transactions on Circuits and Systems II: Express Briefs* **2018**, pp. 1–1. doi:10.1109/TCSII.2018.2865643.
20. Chang, C.; Yuan, Y.; Jiang, T.; Zhou, Z. Field programmable gate array implementation of a single-input fuzzy proportional-integral-derivative controller for DC-DC buck converters. *IET Power Electronics* **2016**, *9*, 1259–1266. doi:10.1049/iet-pel.2015.0688.
21. El Aroudi, A.; Giaouris, D.; Iu, H.H.C.; Hiskens, I.A. A review on stability analysis methods for switching mode power converters. *IEEE Journal on Emerging and Selected Topics in Circuits and Systems* **2015**, *5*, 302–315.
22. Fiore, D.; Hogan, S.J.; di Bernardo, M. Contraction analysis of switched systems via regularization. *Automatica* **2016**, *73*, 279 – 288. doi:https://doi.org/10.1016/j.automatica.2016.06.028.
23. di Bernardo, M.; Fiore, D. Switching control for incremental stabilization of nonlinear systems via contraction theory. 2016 European Control Conference (ECC), 2016, pp. 2054–2059. doi:10.1109/ECC.2016.7810594.
24. Lohmiller, W.; Slotine, J.J.E. On Contraction Analysis for Non-linear Systems. *Automatica* **1998**, *34*, 683 – 696. doi:https://doi.org/10.1016/S0005-1098(98)00019-3.
25. Chen, C.T. *Linear systems theory and design*; Oxford University Press, 1999.
26. Vidyasagar, M. *Nonlinear Systems Analysis*; Prentice Hall, 1993.
27. Slotine, J.J.E.; Li, W. *Applied nonlinear control*; Vol. 199, Prentice hall Englewood Cliffs, NJ, 1991.
28. Khalil, H.K. *Nonlinear control*; Pearson New York, 2015.